Excitonic analysis of many-body effects on the 1*s*-2*p* intraband transition in semiconductor systems

Andrew M. Parks and Marc M. Dignam*
Department of Physics, Engineering Physics and Astronomy Queen's University, Kingston, Ontario, Canada, K7L 3N6

Dawei Wang
Electronic Materials Research Laboratory - Key Laboratory of the Ministry of Education, and International Center for Dielectric Research, Xi'an Jiaotong University, Xi'an 710049, China

(Received 18 February 2013; revised manuscript received 2 May 2013; published 15 May 2013)

We present a detailed study of many-body effects associated with the intraband 1*s*-2*p* transition in two- and three-dimensional photoexcited semiconductors. We employ a previously developed excitonic model to treat effects of exchange and phase space filling (PSF). In this work, we extend the model to include intraband transitions and static free-carrier screening. The exciton transition energies are renormalized by many-body interactions, and the excitonic dynamical equations provide simple expressions for the individual contributions of screening, PSF and exchange. The excitonic model correctly predicts the blue shift and bleaching of the 1*s* exciton resonance due to exchange and PSF. Free-carrier screening is found to enhance these effects by lowering the binding energy of the 1*s* exciton. In contrast, the effects of free-carrier screening on the 1*s*-2*p* transition energy are subtler. For a *coherent* exciton system, in the absence of free-carrier screening, exchange and PSF lead to a blue shift of the transition energy. However, screening decreases the 1*s* binding energy faster than the 2*p* binding energy, which in turn decreases the transition energy. Thus screening effects oppose exchange and PSF, and the overall magnitude and sign of the 1*s*-2*p* transition energy shift depends on the free-carrier density. Specifically, for low to moderate excitation densities, exchange and PSF can be dominated by screening, leading to a net redshift of the transition energy. The results for two- and three-dimensional systems are qualitatively similar, although the magnitude of the shift is much smaller in three dimensions.

DOI: 10.1103/PhysRevB.87.205306 PACS number(s): 78.47.−p, 42.65.Re, 73.21.Cd, 78.67.Pt

I. INTRODUCTION

Various ultrafast optical nonlinear spectroscopy techniques have been applied over the past few decades to probe the many-body dynamics of a wide variety of semiconductor structures. These techniques include nonlinear absorption,[1,2] optical pump-probe spectroscopy,[3–5] degenerate four wave mixing[1,6,7] and two-dimensional Fourier transform spectroscopy.[8] These techniques generally probe changes in the energy states of the carriers by using optical pulses to create or observe the recombination of bound and/or unbound excitons. There are, however, relatively few techniques that directly probe transitions between different excitonic states (intraexcitonic transitions). It is these transitions that are the focus of this work.

With the development of intense terahertz (THz) pulses, researchers have begun to investigate many-body effects in semiconductors using linear and nonlinear terahertz spectroscopy. In undoped systems, a promising technique is to pump with an optical pulse across the band gap and probe with a terahertz pulse.[9–11] The optical pulse creates bound or unbound excitons, and the terahertz pulse probes the transitions between the excitonic states.

If an exciting optical pulse is sufficiently spectrally narrow and is tuned to a specific bound excitonic resonance (e.g., the 1*s* exciton), then at low to moderate intensities, the majority of photoinjected carriers will be excitons in that excitonic state. However, since an exciton is a composite particle, it effectively occupies a region of the electron-hole state space that cannot accommodate additional excitons without violating the Pauli exclusion principle. Thus, as the intensity of the optical pulse increases, additional photoexcited carriers must occupy other states. This phenomenon is referred to as phase space filling (PSF). When the exciting laser is tuned to the ground-state exciton resonance, PSF leads to a blue shift and bleaching of the exciton absorption peak.[3–5,12,13] At higher intensities such that the carrier density approaches the Mott density, PSF will resonantly scatter the ground-state excitons into excited bound and unbound excitonic states.[12,13]

There are, of course, other many-body effects that can affect excitonic transitions. The exchange interaction between electrons and holes provides an effective attraction between excitons, which tends to decrease the exciton energy. Since the total carrier density depends on the intensity of the exciting optical pulse, the density-dependent shift of the transition energy is a nonlinear many-body optical effect. For the 1*s* excitonic absorption resonance, it is known that PSF dominates over exchange, leading to a blue shift of the transition energy.[3–5,12,14] Moreover, it is expected that free-carrier and excitonic screening has a small impact on the energy of this transition for moderate carrier densities.[5] The dependence of the intraband 1*s*-2*p* transition energy on exciton density, however, has only recently attracted significant attention.[9–11] In particular, the influence of free-carrier screening has not been thoroughly characterized experimentally or theoretically.

Interband transitions to optically active excitonic states (*s* states) are driven by optical fields at near infrared (NIR) frequencies. Quantum-mechanical selection rules prohibit interband transitions involving states with nonzero orbital angular momentum (e.g., *p* states). However, these optically forbidden exciton states can be populated by *intraband* transitions (i.e., transitions between exciton subband states), by applying a terahertz (THz) pulse. Thus optical-pump, terahertz-probe

spectroscopy[9–11] can be used to study nonlinearities associated with the intraband $1s$-$2p$ excitonic transition. Since the terahertz absorption is proportional to the density of $1s$ excitons, optical-pump terahertz-probe spectroscopy can provide a direct measurement of the density of $1s$ excitons, as well as the behavior of the $1s$ and $2p$ exciton energies. Although there are a few experimental studies of these intraband transitions,[9,10,15] the technical challenges of producing timed, resonant terahertz pulses has limited the number and scope of such experiments.

To achieve exciton condensation (and exciton-polariton condensation), the static properties of photoexcited semiconductor systems have attracted much investigation[16–21] and mean-field theory is often used as the theoretical tool.[22–24] Investigating the dynamics of photoexcited semiconductor systems is more challenging and a number of theoretical approaches have been developed. The most general approach is to employ quantum kinetic equations using nonequilibrium Green's functions.[25,26] However, such calculations can be cumbersome, and they do not always provide an intuitive description of the interactions. On the other hand, density matrix approaches can provide simple dynamical equations to determine the carrier distributions and polarization. However, this leads to an infinite hierarchy of dynamical equations, which must be truncated by introducing some approximations.

One approach to truncate the density matrix hierarchy is to perform perturbation theory in the optical field.[25] This is a well-controlled approximation, but it is limited to low densities and cannot be used to examine effects such as density-dependent shifts of excitonic absorption peaks. Alternatively, one can factorize expectation values of multiple electron and hole creation and annihilation operators using the random phase approximation, which leads to the well-known semiconductor Bloch equations (SBEs).[25,27] The SBEs have long been used to model interband dynamics in photoexcited semiconductors[1,25] and have the advantage that they are nonperturbative in the optical field. However, the SBEs generally fail to describe intraband coherences[13,28,29] adequately. More general truncation schemes, such as cluster expansions[30] or the dynamic truncation scheme[31] can account for coherences up to arbitrary order, but the resulting dynamical equations can quickly become numerically intractable.

We note that the SBEs and their generalizations represent interactions using a basis of fermionic (i.e., electron and hole) operators. Since intraexcitonic correlations (electron-hole correlations within an exciton) are fundamental to the nonlinear response of semiconductors near the band gap,[1,32] it is more natural to treat the optical and terahertz response of photoexcited semiconductor structures by employing an excitonic basis rather than an electron-hole basis. This is the approach that we take in this paper.

There have been a number of authors who have employed an excitonic approach to treat exciton dynamics in semiconductors.[33–36] We have discussed the relation of those approaches to our approach in previous work.[13,41] The main difficulty deals with the fact that there is no unique way in which to map electron-hole pair states onto exciton states. Some authors deal with this problem by only considering $1s$ excitons, but with all possible center of mass momenta.[33,34] However, as we are interested in transitions to higher internal excitonic states, this is not appropriate to our problem. Perhaps the method that most closely resembles our approach is that of Combescot and co-workers.[35,36] Over a relatively large number of papers, they have developed a method of treating the composite nature of excitons. In agreement with our findings, they point out that it is not possible to derive an excitonic Hamiltonian that treats the effects of direct and exchange interactions as well as the effects of phase-space filling. To our knowledge, however, they have not applied their formalism to the problem of the terahertz response of excitons, which is the main focus of this paper.

Over the course of a number of papers,[13,37–41] we have developed a set of dynamic equations in an excitonic basis that include the effects of PSF and exchange,[13,28] and in asymmetric systems also include the dipole-dipole interaction between excitons.[38,39] We start from the usual electron-hole semiconductor Hamiltonian[25] and employ the Usui transformation[28,37] to project the Hamiltonian onto a basis of quasibosonic pair operators. Using the Heisenberg equation of motion, we obtain a hierarchy of dynamical equations for expectation values of pair operators. We transform these equations to a true (correlated) excitonic basis using a unitary transformation. This basis offers a number of important advantages when bound excitons are dominant (as in the study of resonant excitonic excitation). Unlike the SBEs, the excitonic model treats intraband coherences in an unfactorized form,[28] which is crucial for the $1s$-$2p$ transition. In addition, for low to moderate excitation densities, a numerical simulation of the excitonic dynamical equations is typically more efficient than the SBEs.[13,28] Lastly, the excitonic model provides a clear and intuitive description of interaction involving excitons. We obtain simple, analytic expressions quantifying nonlinear effects without having to perform computationally intensive self-energy calculations.[42]

In this paper, we apply the excitonic model to calculate the density-dependent shift in the $1s$ exciton creation energy and $1s$-$2p$ exciton transition energy in 2D and 3D GaAs systems for optical pulses that resonantly create $1s$ excitons. In both 2D and 3D, we obtain a blue shift of the energy that comes mostly from PSF but has an additional contribution from free-carrier screening. In contrast, in the absence of free-carrier screening, in optical-pump, terahertz-probe experiments where the terahertz pulse delay is less than the interband dephasing time, we obtain a blue shift in the $1s$-$2p$ transition energy, but in both 2D and 3D, if the free-carrier pair density is greater than 5% of the $1s$ exciton density, the transition becomes red shifted.

The paper is organized as follows. In Sec. II, we present the excitonic dynamic equations and discuss the factorization scheme we employ to truncate the hierarchy of equations. In Sec. II A, we show how these equations can be used to obtain the density-dependent exciton transition energies and the $1s$-$2p$ intraexcitonic transition energy. In Sec. III, we describe the model we employ to treat the effects of free-carrier screening on the transition energies. In Sec. IV, we present the results of our calculations and we give our conclusions in Sec. V.

II. EXCITONIC DYNAMICAL EQUATIONS

Much of the formalism presented in this section has been discussed in detail in our previous work.[13,28,37,41] Here, we only outline the key results and concentrate on the new aspects to

the formalism: the effects of screening, exchange, and PSF on the response to terahertz fields.

We start from the familiar semiconductor Hamiltonian[13,25]

$$\mathcal{H}_{\text{s.c.}} = \mathcal{H}_0 + \mathcal{V}_{e-e} + \mathcal{V}_{h-h} + \mathcal{V}_{e-h} + \mathcal{H}_I, \tag{1}$$

where $\mathcal{H}_0$ represents the one-body energies of electrons and holes, $\mathcal{V}_{e-e}$, $\mathcal{V}_{h-h}$, and $\mathcal{V}_{e-h}$ are electron-electron, hole-hole, and electron-hole Coulomb interactions, and $\mathcal{H}_I$ is the interaction Hamiltonian between the carriers and the optical and terahertz electric fields. We project this Hamiltonian onto a basis of pair operators using the Usui transformation.[13,28,37,43] This transformation is not unitary, and must be augmented with a suitable electron-hole pairing operator. For optically excited direct-gap semiconductors, it is natural to employ a pairing scheme matching electrons and holes with opposite momenta, such that the total pair crystal momentum is zero. This transformation introduces the electron-hole-pair creation (annihilation) operator, $B_{\boldsymbol{k}}^\dagger$ ($B_{\boldsymbol{k}}$), which creates (destroys) an electron with crystal momentum $\hbar\boldsymbol{k}$ and a hole with crystal momentum, $-\hbar\boldsymbol{k}$. The commutation relation for these operators is[13,37]

$$[B_{\boldsymbol{k}}, B_{\boldsymbol{k}'}^\dagger] = \delta_{\boldsymbol{k},\boldsymbol{k}'}(1 - 2B_{\boldsymbol{k}}^\dagger B_{\boldsymbol{k}}), \tag{2}$$

which is identical to the canonical bosonic commutation relation, $[B_{\boldsymbol{k}}, B_{\boldsymbol{k}'}^\dagger] = 0$, when $\boldsymbol{k} \neq \boldsymbol{k}'$ but is given by a fermionic anticommutation relation, $\{B_{\boldsymbol{k}}, B_{\boldsymbol{k}}^\dagger\} = 1$, when $\boldsymbol{k} \neq \boldsymbol{k}'$. We thus refer to the electron-hole pairs as quasibosons (qbosons). We note that the fermionic nature of the qbosons is also reflected in the identity

$$B_{\boldsymbol{k}} B_{\boldsymbol{k}} = 0. \tag{3}$$

Applying the Usui transformation to the electron-hole Hamiltonian of Eq. (1), we obtain the qboson Hamiltonian

$$\tilde{\mathcal{H}}_{\text{s.c.}} = \mathcal{H}_Q + \mathcal{V}_X + \tilde{\mathcal{H}}_I, \tag{4}$$

where $\mathcal{H}_Q$ is the energy of a noninteracting qboson pair, $\mathcal{V}_X$ is the Coulomb interaction between qbosons, and $\tilde{\mathcal{H}}_I$ accounts for interactions between qbosons electric fields (optical and terahertz). Evaluating the Heisenberg equation of motion, the qboson operators are found to satisfy the dynamical equation[13]

$$\begin{aligned} i\hbar\frac{d}{dt}B_{\boldsymbol{p}}^\dagger = &-E_{\boldsymbol{p}}^0 B_{\boldsymbol{p}}^\dagger + \sum_{\boldsymbol{k}} V_{\boldsymbol{p}-\boldsymbol{k}} B_{\boldsymbol{k}}^\dagger \\ &+ 2\sum_{\boldsymbol{k}} V_{\boldsymbol{p}-\boldsymbol{k}}(B_{\boldsymbol{p}}^\dagger B_{\boldsymbol{k}}^\dagger B_{\boldsymbol{k}} - B_{\boldsymbol{k}}^\dagger B_{\boldsymbol{p}}^\dagger B_{\boldsymbol{p}}) \\ &+ \boldsymbol{E}_{\text{opt}}(t)\cdot\boldsymbol{d}_{cv}(1 - 2B_{\boldsymbol{p}}^\dagger B_{\boldsymbol{p}}) \\ &+ \sum_{\boldsymbol{k}} \boldsymbol{E}_{\text{THz}}(t)\cdot\boldsymbol{G}_{\boldsymbol{k}\boldsymbol{p}} B_{\boldsymbol{k}}^\dagger(1 - 2B_{\boldsymbol{p}}^\dagger B_{\boldsymbol{p}}), \end{aligned} \tag{5}$$

where $E_{\boldsymbol{p}}^0$ is the kinetic energy of a qboson with relative momentum $\hbar\boldsymbol{k}$, $V_{\boldsymbol{p}-\boldsymbol{k}}$ is the (screened) Coulomb interaction in the momentum representation, $\boldsymbol{d}_{cv}$ is the interband transition amplitude, $\boldsymbol{G}_{\boldsymbol{k}\boldsymbol{p}}$ are the intraband transition matrix elements, and $\boldsymbol{E}_{\text{opt}}(\boldsymbol{E}_{\text{THz}})$ is the optical (terahertz) electric field.

To proceed, one could use Eq. (5) and the corresponding equation for $B_{\boldsymbol{p}}^\dagger B_{\boldsymbol{q}}$ to obtain expressions for the evolution of the expectation values of the interband and intraband polarizations. Using the random phase approximation (RPA), we have shown that these equations, in fact, reduce to the semiconductor Bloch equations.[41] However, as discussed in the previous section, the SBEs are not generally appropriate for the treatment of the intraband polarization arising from excitons. If one does not apply the RPA, the resulting set of equations becomes very difficult to employ as the basis set of free carriers is generally very large for 2D or 3D systems and truncating the hierarchy of equations is difficult, particularly in treating both interband and intraband dynamics as one cannot assume rotational symmetry.[31,44]

Using the fact that the response of the system is dominated by a few excitonic states, we can simplify the equations by transforming from the qboson basis to the true excitonic basis through the unitary transformation

$$B_\mu^\dagger = \sum_{\boldsymbol{k}} \varphi_{\boldsymbol{k}}^\mu B_{\boldsymbol{k}}^\dagger; \quad B_{\boldsymbol{k}}^\dagger = \sum_\mu \varphi_{\boldsymbol{k}}^{\mu *} B_\mu^\dagger, \tag{6}$$

where $\varphi_{\boldsymbol{k}}^\mu$ is the momentum-space envelope function[13] for an exciton in state μ, which is related to the configuration space envelope function by

$$\varphi^\mu(\boldsymbol{r}) = \sum_{\boldsymbol{k}} \varphi_{\boldsymbol{k}}^\mu e^{i\boldsymbol{k}\cdot\boldsymbol{r}}. \tag{7}$$

Using Eqs. (2) and (6), it is easily shown that the commutation relations for the excitonic operators are

$$[B_\mu, B_\nu] = 0, \quad [B_\mu, B_\nu^\dagger] = \delta_{\mu,\nu} - 2\sum_{\gamma_1,\gamma_2} \chi_{\gamma_1,\gamma_2}^{\mu,\nu} B_{\gamma_1}^\dagger B_{\gamma_2}, \tag{8}$$

where

$$\chi_{\gamma_1,\gamma_2}^{\mu,\nu} \equiv \sum_{\boldsymbol{k}} \varphi_{\boldsymbol{k}}^{\mu *}\varphi_{\boldsymbol{k}}^\nu \varphi_{\boldsymbol{k}}^{\gamma_1 *}\varphi_{\boldsymbol{k}}^{\gamma_2}. \tag{9}$$

In the limit of vanishing excitonic density, these are simply bosonic commutation relations. Note that, in general, the excitonic states can be bound or unbound states, but the approach is most efficient when the response is dominated by bound excitons.

As we have discussed in earlier work,[41] applying the above unitary transformation directly to the qboson Hamiltonian and then deriving the Heisenberg equations of motion does not yield the correct result because this procedure effectively neglects the relation, $B_{\boldsymbol{k}} B_{\boldsymbol{k}} = 0$. This is in agreement with the findings of Combescot *et al.*.[36] Instead, we apply the excitonic transformation to the dynamic equation (5) and obtain

$$\begin{aligned} &i\hbar\frac{d}{dt}B_\mu^\dagger + E_\mu B_\mu^\dagger \\ &\quad = 2\sum_{\{\gamma_j\}} R_{\gamma_1,\gamma_2,\gamma_3}^\mu B_{\gamma_1}^\dagger B_{\gamma_2}^\dagger B_{\gamma_3}, \\ &\qquad + \boldsymbol{E}_{\text{opt}}(t)\cdot\boldsymbol{d}_{cv}\left(C_\mu - 2\sum_{\{\gamma_j\}} C_{\mu,\gamma_1,\gamma_2} B_{\gamma_1}^\dagger B_{\gamma_2}\right) \\ &\qquad + \boldsymbol{E}_{\text{THz}}(t)\cdot\sum_\gamma \boldsymbol{G}_{\mu,\gamma} B_\gamma^\dagger \\ &\qquad + \boldsymbol{E}_{\text{THz}}(t)\cdot\sum_{\{\gamma_j\}} \boldsymbol{G}_{\gamma_4,\gamma_5} T_{\gamma_1,\gamma_2,\gamma_3,\gamma_4\gamma_5}^\mu B_{\gamma_1}^\dagger B_{\gamma_2}^\dagger B_{\gamma_3}, \end{aligned} \tag{10}$$

where $\sum_{\{\gamma_j\}} \equiv \sum_{\gamma_1,\gamma_2\ldots}$. The R coefficients account for exchange and PSF interactions and are given by

$$R^{\mu}_{\gamma_1,\gamma_2,\gamma_3} \equiv X^{\mu}_{\gamma_1,\gamma_2,\gamma_3} + P^{\mu}_{\gamma_1,\gamma_2,\gamma_3}, \tag{11}$$

where the component

$$X^{\mu}_{\gamma_1,\gamma_2,\gamma_3} \equiv \sum_{\boldsymbol{k},\boldsymbol{p}} V_{\boldsymbol{p}-\boldsymbol{k}} \varphi^{\mu}_{\boldsymbol{p}} \varphi^{\gamma_1 *}_{\boldsymbol{p}} \varphi^{\gamma_2 *}_{\boldsymbol{k}} \varphi^{\gamma_3}_{\boldsymbol{k}} \tag{12}$$

arises from the exchange interaction, and

$$P^{\mu}_{\gamma_1,\gamma_2,\gamma_3} \equiv -\sum_{\boldsymbol{k},\boldsymbol{p}} V_{\boldsymbol{p}-\boldsymbol{k}} \varphi^{\mu}_{\boldsymbol{p}} \varphi^{\gamma_1 *}_{\boldsymbol{k}} \varphi^{\gamma_2 *}_{\boldsymbol{p}} \varphi^{\gamma_3}_{\boldsymbol{p}} \tag{13}$$

is due to phase space filling. The coefficient

$$C_{\mu} \equiv \sum_{\boldsymbol{k}} \varphi^{\mu}_{\boldsymbol{k}} = \varphi^{\mu}(\boldsymbol{r}=0), \tag{14}$$

gives the contribution of the excitonic envelope function to the interband (optical) dipole matrix element, and

$$C_{\mu,\gamma_1,\gamma_2} = \sum_{\boldsymbol{k}} \varphi^{\mu}_{\boldsymbol{k}} \varphi^{\gamma_1 *}_{\boldsymbol{k}} \varphi^{\gamma_2}_{\boldsymbol{k}} \tag{15}$$

describes the optical spectral hole burning effect. The terahertz dipole matrix element between excitonic states is given by

$$\boldsymbol{G}_{\mu\gamma} = -e \int d\boldsymbol{r} \varphi^{\mu *}(\boldsymbol{r}) \boldsymbol{r} \varphi^{\gamma}(\boldsymbol{r}), \tag{16}$$

while the terahertz spectral hole burning coefficient is given by

$$T^{\mu}_{\gamma_1,\gamma_2,\gamma_3,\gamma_4\gamma_5} = \sum_{\boldsymbol{k},\boldsymbol{p}} \varphi^{\mu}_{\boldsymbol{p}} \varphi^{\gamma_1 *}_{\boldsymbol{k}} \varphi^{\gamma_2 *}_{\boldsymbol{p}} \varphi^{\gamma_3}_{\boldsymbol{p}} \varphi^{\gamma_4}_{\boldsymbol{k}} \varphi^{\gamma_5 *}_{\boldsymbol{p}}. \tag{17}$$

In this excitonic basis, the interband polarization is given by

$$\boldsymbol{P}_{\text{inter}} = \frac{\boldsymbol{d}_{cv}}{V} \sum_{\mu} C_{\mu} \langle B^{\dagger}_{\mu} \rangle + \text{c.c.}, \tag{18}$$

while the intraband polarization is given by

$$\boldsymbol{P}_{\text{intra}} = \frac{1}{V} \sum_{\mu,\nu} \boldsymbol{G}_{\mu\nu} \langle B^{\dagger}_{\mu} B_{\nu} \rangle, \tag{19}$$

where V is the volume of the system. Thus, to compute the optical and terahertz response of the system, we need to determine the dynamics of the interband and intraband coherence functions, $\langle B^{\dagger}_{\mu} \rangle$and $\langle B^{\dagger}_{\mu} B_{\nu} \rangle$. Taking the expectation value of Eq. (10) gives the excitonic dynamical equations (EXEs) for the interband coherence function $\langle B^{\dagger}_{\mu} \rangle$. This equation will include terms containing three operator coherence functions, $\langle B^{\dagger}_{\gamma_1} B^{\dagger}_{\gamma_2} B_{\gamma_3} \rangle$, which require their own dynamic equations. This leads to an infinite hierarchy of dynamical equations, which must be truncated. To truncate this, we will need to factorize the coherence functions with three or more operators. We have shown in previous work[41] that with the appropriate factorization and working in the coherent limit, these equations give essentially identical results to the semiconductor Bloch equations. In this work, we will not present a general factorization scheme for the dynamic equations for the interband and intraband coherence functions. Rather, we will present factorization schemes specific to the problem of determining the density-dependent shifts in the optical absorption peak for the $1s$ exciton and in the terahertz absorption peak corresponding to the transition from a $1s$ to a $2p$ exciton.

A. Determining the optical and terahertz absorption peak shifts

As we have demonstrated in previous publications, the EXEs can be used to calculate the evolution of the interband[13,38,39,41] and intraband[40,45,46] polarizations for a given optical and terahertz excitation. For a general ultrashort pulse excitation, such calculations can be rather involved, even for a single quantum well.[13] However, if the optical pulse is resonant only on the ground-state $1s$ exciton, and is sufficiently narrow such that the population of excited-state excitons (bound and unbound) is much smaller than the $1s$ exciton population, some simple approximations can be made to obtain the excitonic spectral shifts without having to solve the full dynamic equations.

To determine the shift in the energies of the excitonic states, we begin by taking the expectation value of the intraband dynamic equation (10) for times after the optical pulse has passed, but before any terahertz pulse has arrived. We then obtain

$$i\hbar \frac{d}{dt} \langle B^{\dagger}_{\mu} \rangle = -(E_{\mu} + i\hbar/T_{\mu}) \langle B^{\dagger}_{\mu} \rangle + 2 \sum_{\{\gamma_j\}} R^{\mu}_{\gamma_1,\gamma_2,\gamma_3} \langle B^{\dagger}_{\gamma_1} B^{\dagger}_{\gamma_2} B_{\gamma_3} \rangle, \tag{20}$$

where we have added in a phenomenological interband dephasing time, T_{μ}. Because the optical pulse is resonant on the $1s$ exciton, the resulting exciton population will be dominated by this state. Thus, as an approximation, in the sum on the second line of Eq. (20), we only include terms where $\gamma_3 = 1s$ and either γ_1 or γ_2 is $1s$. Furthermore, because we are interested only in the resonant contribution, we will only consider terms where $\gamma_1 = 1s$ and $\gamma_2 = \mu$, or $\gamma_1 = \mu$ and $\gamma_2 = 1s$. With these approximations, and noting that there is only one term when $\mu = 1s$, we obtain

$$i\hbar \frac{d}{dt} \langle B^{\dagger}_{\mu} \rangle = -(E_{\mu} + i\hbar/T_{\mu}) \langle B^{\dagger}_{\mu} \rangle + (2 - \delta_{\mu,1s}) \big(R^{\mu}_{1s,\mu,1s} + R^{\mu}_{\mu,1s,1s} \big) \langle B^{\dagger}_{\mu} B^{\dagger}_{1s} B_{1s} \rangle. \tag{21}$$

In Appendix A, we show that for optical pulses that are considerably shorter than the interband dephasing time, the system is a coherent state of $1s$ excitons immediately after the optical pulse has passed. Using this, we show that for subsequent excitation by a weak terahertz field, the coherence function can be factorized as

$$\langle B^{\dagger}_{\mu} B^{\dagger}_{1s} B_{1s} \rangle = \langle B^{\dagger}_{\mu} \rangle \langle B^{\dagger}_{1s} B_{1s} \rangle. \tag{22}$$

Using this factorization in Eq. (21), we obtain

$$i\hbar \frac{d}{dt} \langle B^{\dagger}_{\mu} \rangle = -(\varepsilon_{\mu} + i\hbar/T_{\mu}) \langle B^{\dagger}_{\mu} \rangle, \tag{23}$$

where the *renormalized exciton energy* is given by

$$\varepsilon_{\mu} \equiv E_{\mu} - (2 - \delta_{\mu,1s}) \big(R^{\mu}_{1s,\mu,1s} + R^{\mu}_{\mu,1s,1s} \big) N_{1s}, \tag{24}$$

and

$$N_{1s} \equiv \langle B^{\dagger}_{1s} B_{1s} \rangle \tag{25}$$

is the number of 1s excitons.

From Eq. (24), we see that at this level of approximation, the energy of any excitonic state shifts linearly with the 1s exciton density (assuming the R coefficients are constant). Since the density is related to the peak intensity of the exciting optical pulse, the energy shift should depend linearly on the optical intensity. Experimentally, this will manifest itself as a shift of the 1s exciton absorption peak, with the magnitude of the shift depending on the intensity. This equation can be applied to any excitonic state, as long as the 1s excitons are the dominant population. In a previous work,[13] we obtained analytic expressions and numerical values regarding the density induced blue shift and compared to other authors' work.[3,5,42] Our current approach, however, generalizes this to allow us to treat higher excitonic states.

To obtain the density-dependent shift of the 1s-2p terahertz excitonic transition, one has to perform a similar analysis on the intraband equations of motion. We present this intraband analysis in Appendix B, and show that in the limit of a macroscopic system, we obtain a shift that is given simply by

$$E_{2p-1s} = (\varepsilon_{2p} - E_{2p}) - (\varepsilon_{1s} - E_{1s}), \tag{26}$$

which reduces to

$$\Delta E_{2p-1s} = 2\big(R^{1s}_{1s,1s,1s} - R^{2p}_{1s,2p,1s} - R^{2p}_{2p,1s,1s}\big)N_{1s}. \tag{27}$$

The energy shift in the 1s-2p terahertz excitonic transition has been calculated in the absence of screening in a previous work.[47] They obtained a similar result to ours, except in their analysis they assumed that the excitons were *incoherent* and obtained results for the limiting case $R^{2p}_{1s,2p,1s} = 0$. In this work, we are interested in resonant optical excitation with subsequent weak terahertz excitation, and how this process is affected by free-carrier screening in particular. In this situation, the excitonic state is initially a *coherent* state (see Appendix A) and $R^{2p}_{1s,2p,1s}$ is nonzero. Thus our work is complementary to the previous work.[47]

The picture we have described thus far is not quite complete because, even for resonant excitation, there will always be some unbound electron-hole pairs generated via a number of different mechanisms. They could be directly excited by the spectral tail of the optical pulse or they could be indirectly excited via coherent intraexcitonic scattering that occurs at even moderate densities due to PSF and exchange. This second mechanism is represented by the nonresonant terms in the second line of Eq. (20) that we ignored in our energy renormalization analysis. We have included these terms in earlier work and have shown that, even at moderate densities, they can lead to significant excited-state populations.[13] For example, in a GaAs quantum well, we found that for resonant excitation of the 1s excitonic state, approximately 10% of the carriers were unbound electron-hole pairs when the density of 1s excitons was $n_{2D} = 2 \times 10^{10}$ cm^{-2}. Recent experimental studies[9,48] of GaAs/AlGaAs QWs have also demonstrated that even for resonant excitation of the 1s excitons, significant free-carrier populations are generated for moderate to high 1s exciton densities. These photogenerated free carriers will provide screening, which will affect the exciton energies in two ways: (1) screening will decrease the binding energy of the excitons, leading to a redshift in the excitonic energies, and (2) screening will modify the exciton envelope functions, which will change the values for the R coefficients. We treat the effects of screening in the next section.

III. MODEL FOR FREE CARRIER SCREENING

It is well known that the influence of screening due to free carriers is much larger than screening due to the ground-state excitons.[49] In this section, we present our model for the excitonic states in a strictly two-dimensional (2D) system and in three-dimensional (3D) bulk. In both cases, we use the dielectric constant and carrier masses appropriate to GaAs. We choose to model a strictly 2D system rather than a specific quantum well, as this will give us a measure of the density effects in the extreme limit of 2D confinement, while the bulk results give us the other extreme. The 2D system also has the advantage that many of the results are analytic.

To model the free-carrier screening, we employ the random phase approximation (RPA) for the screened dielectric function.[26] This leads to the statically screened Coulomb matrix elements[25]

$$V^{2D}_{\boldsymbol{k}-\boldsymbol{p}}(\kappa) = \frac{e^2/2\epsilon L^2}{|\boldsymbol{k}-\boldsymbol{p}| + \kappa}, \tag{28}$$

for a 2D system, and

$$V^{3D}_{\boldsymbol{k}-\boldsymbol{p}}(\kappa) = \frac{e^2/\epsilon L^3}{|\boldsymbol{k}-\boldsymbol{p}|^2 + \kappa^2} \tag{29}$$

for a 3D system, where L is the linear dimension of the system, which is related to the volume by $V = L^d$, where d is the dimension of the system. The background dielectric constant of the system is ϵ, which is taken to be $\epsilon = 12.5$ in calculations.[49] In the Debye model,[25,49] the screening wave number is given in 2D by

$$\kappa = \frac{e^2}{2\epsilon}\frac{\partial n}{\partial \mu} \tag{30}$$

and in 3D, by

$$\kappa = \sqrt{\frac{e^2}{\epsilon}\frac{\partial n}{\partial \mu}}, \tag{31}$$

where n is the density of the free carriers (i.e., free electrons and holes) and μ is the associated chemical potential. We assume a Fermi-Dirac distribution for the free carriers and use Eqs. (30) and (31) to relate the screening wave number to the free-carrier density. To be concrete, in all calculations, we take the carrier temperature to be $T = 20$ K. Given that the free carriers are optically generated, we take the densities of free electrons and holes (n_{eh}) to be equal. For a two-dimensional system, this leads to the closed-form expression[49]

$$a_0\kappa = \frac{2m_e}{m^*}\left[1 - \exp\left(-\frac{\beta\pi\hbar^2 n_{eh}}{m_e}\right)\right] + \frac{2m_h}{m^*}\left[1 - \exp\left(-\frac{\beta\pi\hbar^2 n_{eh}}{m_h}\right)\right], \tag{32}$$

where m_e (m_h) is the electron (hole) effective mass, and m^* is the exciton reduced mass. In contrast, the screening wave

number for a three-dimensional system must be calculated numerically for a given n_{eh}.

To evaluate the R coefficients of Eq. (11), we need to determine the exciton wave functions in the presence of screening. We do this using a variational approach, where we assume the wave functions have the same functional form as in the unscreened case, but with an effective Bohr radius that is modified by the screened interaction. Specifically, for the wave function of an exciton in the state μ we replace the Bohr radius with the quantity $(\alpha_\mu)^{-1}$, which is treated as a variational parameter (with units of inverse length). As shown by Lee *et al.*,[49] the resulting variational energy is most easily evaluated in configuration space using the effective Hamiltonian

$$H_{\text{eff}} = \frac{p^2}{2m^*} - V_s(\kappa, r), \tag{33}$$

where $V_s(\kappa,r)$ is the screened Coulomb potential. Taking the inverse Fourier-Bessel transform of Eq. (28), and using an integral result due to Watson[50] gives the 2D potential

$$V_s^{\text{2D}}(\kappa,r) = \frac{e^2}{4\pi\epsilon}\left\{\frac{1}{r} - \frac{\pi}{2}\kappa\left[\boldsymbol{H}_0(\kappa r) - N_0(\kappa r)\right]\right\}, \tag{34}$$

where $\boldsymbol{H}$ and N are Struve and Neumann functions, respectively. This expression was quoted by Stern and Howard,[51] and is commonly used to treat two-dimensional systems.[49,52,53] For a three-dimensional system, the inverse Fourier transform of Eq. (29) gives the simple result

$$V_s^{3D}(\kappa,r) = \frac{e^2}{4\pi\epsilon}\frac{e^{-\kappa r}}{r}, \tag{35}$$

which is the familiar Yukawa potential.[26]

Figure 1(a) shows the $1s$ and $2p$ screened-exciton binding energies and variational parameters as a function of free-carrier density for a two-dimensional system. The binding energy, E_μ^b is the exciton energy relative to the band-edge energy at zero electron-hole density. The discontinuity in the plot for α_{2p} shows that the $2p$ state becomes unbound at a finite free-carrier density (corresponding to $a_0\kappa \simeq 0.29$). It is well known that the $1s$ binding energy remains nonzero for a 2D system, regardless of the screening density.[49] For a 3D system, Fig. 1(b) shows that both the $1s$ and $2p$ states become unbound for a finite level of screening. Figure 1 also shows that, for a given free-carrier density, the decrease in the magnitude of the exciton binding energy is greater for the $1s$ state (provided the $2p$ state remains bound). This means that the effects of free-carrier screening on the exciton binding energies will tend to *decrease* (redshift) the $1s$-$2p$ transition energy. In the next section, we examine the dependence of the transition energies on carrier density when the effects of exchange and PSF are also included.

Before closing this section, we note that we use the term "binding energy" to refer to the difference between the zero-density band gap and the energy of the screened exciton. Of course, both free carriers and excitons can lead to a renormalization of the band gap and so due to the shift in the band edge, the observed binding energy will not be E_μ^b. However, the excitonic energies that we will finally calculate will correspond to the transition energies measured in experiment, which is the quantity that we are after. To simplify

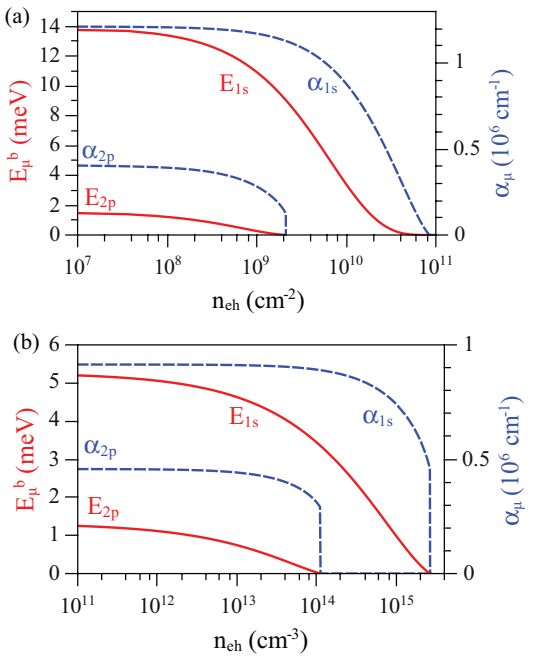

FIG. 1. (Color online) Calculated variational parameter α_μ (dashed) and screened-exciton binding energy E_μ^b (solid) for the exciton states $\mu = 1s, 2p$ in (a) 2D and (b) 3D systems.

the discussion, in all that follows, we will call the quantity E_μ^b the screened-exciton binding energy.

IV. RESULTS

We will now calculate the effect of the $1s$ exciton density on the $1s$ exciton interband and $1s$-$2p$ intraband transitions due to the combination of free-carrier screening, PSF, and exchange. Using Eq. (24) to model resonant excitation of the $1s$ exciton, the renormalized exciton energies may be written as

$$\varepsilon_\mu = E_\mu - \frac{e^2 a_0}{\epsilon}(2 - \delta_{\mu,1s})\left(\bar{R}^\mu_{\mu,1s,1s} + \bar{R}^\mu_{1s,\mu,1s}\right)n_{1s}, \tag{36}$$

where $E_\mu(<0)$ is the exciton energy relative to the zero-density band gap, n_{1s} is the density of $1s$ excitons, and we have introduced the dimensionless R coefficient,

$$\bar{R}^\mu_{\gamma_1,\gamma_2,\gamma_3} = \frac{\epsilon L^D}{e^2(a_0)^{D-1}} R^\mu_{\gamma_1,\gamma_2,\gamma_3}, \tag{37}$$

for a D-dimensional system. Recall that $R^\mu_{\gamma_1,\gamma_2,\gamma_3}$ is given by Eqs. (11)–(13), with $V_{\boldsymbol{k}-\boldsymbol{p}}$ being the screened Coulomb interaction given by Eq. (28) in 2D and Eq. (29) in 3D. Note that both the screened energy E_μ and the R coefficients depend on the level of screening. Thus, if the free-carrier density is constant (i.e., $\partial n_{eh}/\partial n_{1s} = 0$), we see from Eq. (36) that the exciton energy will vary linearly n_{1s}. Of course, n_{eh} and n_{1s} are not necessarily independent, but it is instructive to consider first the influence of screening independently from PSF and exchange. We will then consider the case where the free-carrier density is proportional to the density of $1s$ excitons (i.e., $n_{eh}/n_{1s} = \text{const}$), which is more relevant for experiments where the excitonic transition energies are measured as a function of laser intensity.

A. 1*s* interband transition

In this section, we examine the 1*s* interband transition energy in 2D and 3D systems. There have been a number of previous authors who have examined shifts of the excitonic energy level as a function of carrier density.[13,36,41,42,54] These have ranged from quasi-1D[41,54] and 2D[13,42] systems to 3D systems.[36] Some have examined the effects of just 1*s* excitons on the shift of the 1*s* excitons themselves,[13,42] while others have examined the effects of free carriers on the 1*s* excitonic transitions.[54] In this section, to set the stage for our calculation of the shifts in the 1*s* to 2*p* intraband transitions, we examine the effects of a moderate 1*s* exciton density in combination with a small density of free carriers on the shifts in the 1*s* excitons in both 2D and 3D systems.

We present results for 1*s* exciton densities that are less than $n_{1s} = 10^{10}$ cm^{-2} in 2D and $n_{1s} = 10^{15}$ cm^{-3} in 3D. We are restricting ourselves to these densities for several reasons. First, when we are using proportional screening, we want to stay in the range of free-carrier densities for which the 2*p* exciton remains bound. From Fig. 1, we see that in 2D (3D), this means that we must have $n_{eh} < 2 \times 10^9$ cm^{-2} ($n_{eh} < 10^{14}$ cm^{-3}). Second, because this is an excitonic model, we want to stay well below the density where there is strong spatial overlap between the 1*s* excitons, for then a significant portion of the excitons will become ionized and an excitonic approach becomes inappropriate. As discussed earlier, in a GaAs quantum well, we find that for resonant excitation of 1*s* excitons, approximately 10% of the generated carriers are unbound when the density is $n_{2D} = 2 \times 10^{10}$ cm^{-2}. A simple estimate of an appropriate maximum exciton density is the density at which the average separation between excitons is ten times their radius (where the radius is taken to be the radius of maximum probability density). For GaAs in 2D, this gives a density of $n_c \simeq 3 \times 10^9$ cm^{-2}, while in 3D it gives $n_c \simeq 2 \times 10^{14}$ cm^{-3}. As these are rather conservative estimates, we go to somewhat higher densities than these in both 2D and 3D.

When there are no free carriers, we find that in 2D, $\bar{X}^{1s}_{1s,1s,1s} \simeq 0.3795$, while $\bar{P}^{1s}_{1s,1s,1s} \simeq -0.5000$, which gives a net R coefficient of $\bar{R}^{1s}_{1s,1s,1s} \simeq -0.1205$. Thus the effect of exchange is to lower the energy, while the effect of PSF is to increase the energy. Because the PSF effect is slightly larger, we obtain a net blue shift that is consistent with experimental results for quantum wells.[3,5] Our result is also in agreement with the SBE-based result presented in Ref. 42.

Figure 2(a) shows the renormalized 1*s* exciton energy in the 2D system relative to the zero-density band gap as a function of the (photoexcited) 1*s* density for various fixed free-carrier densities. From Eq. (36), we know that the slope of the linear blue shift is determined by the R coefficient, which embodies effects of PSF and exchange. For moderate 1*s* densities (10^9–10^{10} cm^{-2}) the total shift is about 0.6 meV. The offsets of the curves in Fig. 2(a) are determined by E_μ in Eq. (36), the value of which is affected solely by free-carrier screening. In principle, the R coefficients depend on the level of screening (see Appendix C 2). However, the slopes of the four curves in Fig. 2 are almost identical, which means the dependence is very weak over the range of densities considered. As is shown in Appendix C 2, the difference in

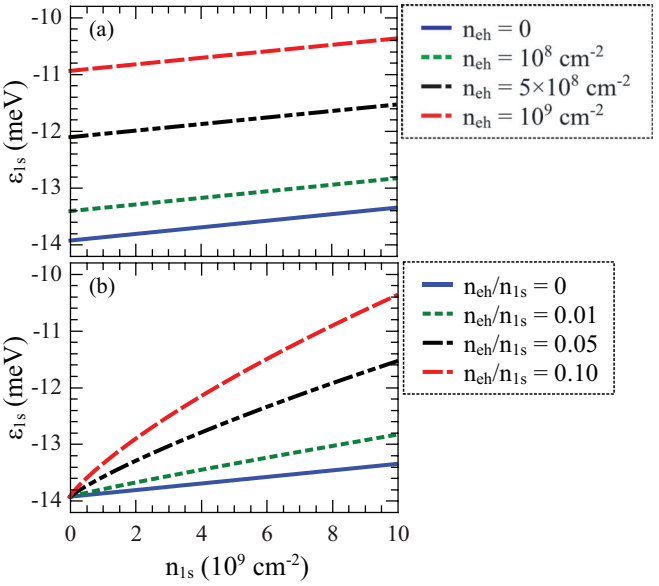

FIG. 2. (Color online) Renormalized 1*s* exciton energy for a 2D system relative to the zero-density band edge. The exciton energy is plotted as a function of the n_{1s} when the free-carrier density is (a) constant, (b) proportional to n_{1s}.

the slopes for no free carriers and $n_{eh} = 10^9$ cm^{-2} is only 1.4%. Thus the main contribution of free-carrier screening to the renormalized 1*s* interband transition energy is through the decrease in the screened-exciton binding energy, E^b_{1s}, which reinforces the blue shift due to PSF and exchange.

We now consider the more experimentally relevant situation where the free-carrier density increases with the 1*s* exciton density. To be concrete, we assume that the free-carrier density is simply proportional to the 1*s* exciton density, which is valid for direct excitation and is a reasonable model for moderate excitation densities. Figure 2(b) shows ε_{1s} as a function of n_{1s} for several values of n_{eh}/n_{1s}. We see here that free-carrier screening greatly enhances the blue shift, and that this shift is still essentially linear. In the case that 10% of the carriers are free carriers, 84% of the shift is due to free-carrier screening.

For 3D systems, we obtain qualitatively similar results to what we obtained in 2D, although the overall magnitude of the blue shift is considerably smaller. When there are no free carriers, we find that $\bar{X}^{1s}_{1s,1s,1s} \simeq 2.083$, while $\bar{P}^{1s}_{1s,1s,1s} \simeq -2.625$, leading to a net R coefficient of $\bar{R}^{1s}_{1s,1s,1s} \simeq -0.542$. This result agrees to first order in the density to the result presented in Eq. (7.80) of Ref. 36.

Again, the effect of exchange is to lower the energy, while the effect of PSF is to increase the energy and we obtain a small net blue shift. Indeed, Fig. 3(a) shows that the blue shift due to PSF and exchange combined is only ~0.2 meV for moderate 1*s* densities (10^{14}–10^{15} cm^{-3}). This is consistent with experimental and theoretical results in bulk GaAs for resonant excitation at low temperature, which found very small shifts of less than 0.1 meV.[55] A number of other experimental studies have focused on the 1*s* blue shift as a function of the well width in GaAs/AlGaAs quantum wells; they generally demonstrate a vanishingly small shift beyond some finite width.[5,12] A more recent study has demonstrated a small shift of the 1*s* energy in bulk ZnSe,[14] which they theoretically

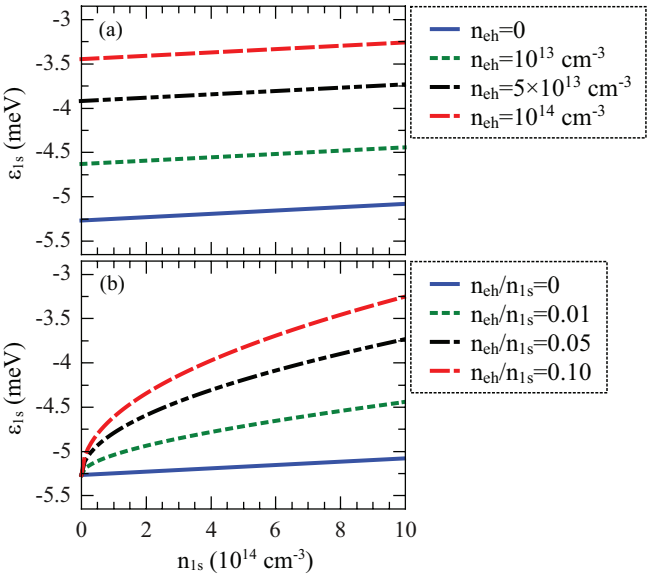

FIG. 3. (Color online) Renormalized $1s$ exciton energy for a 3D system relative to the zero-density band edge. The exciton energy is plotted as a function of n_{1s} when the free-carrier density is (a) constant and (b) proportional to n_{1s}.

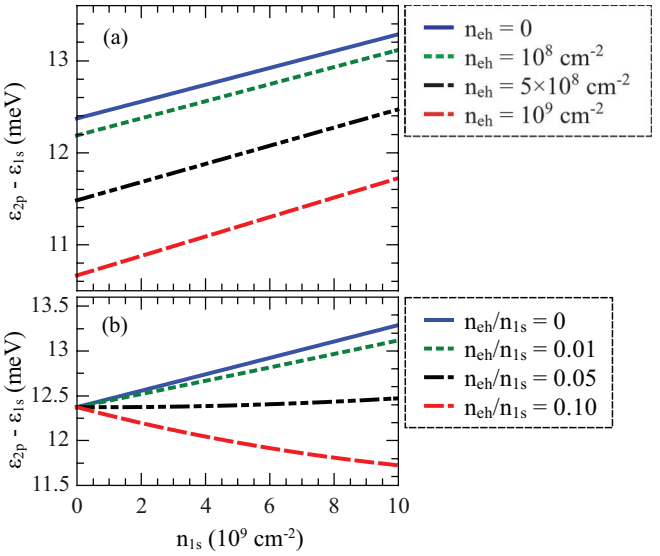

FIG. 4. (Color online) Renormalized $1s$-$2p$ transition energy for a 2D system. The transition energy is plotted as a function of the n_{1s} when the free-carrier density is (a) constant and (b) proportional to n_{1s}.

attributed to screening. Note that it has previously been shown theoretically[56] that free-carrier screening does result in a blue shift in the exciton energy in both 2D and 3D, which is again consistent with our results.

B. $1s$-$2p$ intraexcitonic transition

The expression for the renormalized $1s$-$2p$ intraexcitonic transition energy is given by

$$\varepsilon_{2p} - \varepsilon_{1s} = E_{2p} - E_{1s} - \frac{2e^2 a_0}{\epsilon}\left(\bar{R}^{2p}_{2p,1s,1s} + \bar{R}^{2p}_{1s,2p,1s} - \bar{R}^{1s}_{1s,1s,1s}\right) n_{1s}. \quad (38)$$

The calculated values for the R coefficients in the absence of screening are presented in Table I of Appendix C 2. The R coefficients are quite insensitive to variations in n_{eh} (see Appendix C 2), which means the E_μ are the only terms on the right-hand side of Eq. (38) affected significantly by screening. Thus, for a constant free-carrier density ($\partial n_{eh}/\partial n_{1s} = 0$), Eq. (38) describes a linear shift with the slope determined by the R coefficients. Figure 4(a) shows the $1s$-$2p$ transition energy for a two-dimensional system at different values of n_{eh}. The positive slope indicates that PSF and exchange impart a small blue shift. However, the transition energy decreases as the level of screening increases, as evidenced by the negative offsets of the plots in Fig. 4. This is due to the decreased difference in the screened exciton energies ($E_{2p} - E_{1s}$) observed previously in Sec. III. Thus the overall shift of the renormalized $1s$-$2p$ transition energy is determined by the competing effects of screening and PSF and exchange.

In Fig. 4(b), we show the renormalized transition energy for the case of proportional screening. If $(n_{eh}/n_{1s}) \gtrsim 5\%$, screening dominates exchange and PSF, leading to a linear *red* shift of the transition energy. Similar behavior is observed for a three-dimensional system, as shown in Fig. 5. Although the precise relationship between the density of free carriers and excitons is difficult to determine exactly, it is clear that the effects of free-carrier screening can be significant for intraband transitions. Focussing on the 2D system, Fig. 4 shows a redshift of approximately -6.5×10^{-11} meV cm^2 when $n_{eh}/n_{1s} = 10\%$. One experimental study of the $1s$-$2p$ transition in GaAs/AlGaAs quantum wells[9] found evidence supporting a proportional model for the free-carrier density when the system free-carrier density is much less than the $1s$ exciton density. The authors reported a redshift of the transition energy that is given approximately by -1.75×10^{-11} meV cm^2. However, a similar study[10] found a much smaller redshift in GaAs/AlGaAs quantum wells, and a vanishing shift in GaInAs/GaAs quantum wells. Despite the apparent discord, one consistent inference of these studies was the suspected role of free-carrier screening. These conflicting results certainly motivate further study—ideally focusing on the moderate excitation regime and *coherent* excitons,[57] with a careful analysis of free-carrier screening. It should be noted that the existing experimental studies[9,10] have focused on the high density regime (i.e., approaching total ionization), where the

TABLE I. Values for the components of the R coefficients.

Dimensionless coefficient	Calculated value 2D	3D
$\bar{X}^{1s}_{1s,1s,1s}$	0.3795	2.083
$\bar{P}^{1s}_{1s,1s,1s}$	−0.5000	−2.625
$\bar{X}^{2p}_{2p,2p,1s}$	0.5264	3.338
$\bar{P}^{2p}_{2p,1s,1s}$	−0.1495	−1.665
$\bar{X}^{2p}_{1s,2p,1s}$	0.1468	1.601
$\bar{P}^{2p}_{1s,2p,1s}$	−0.8356	−4.760

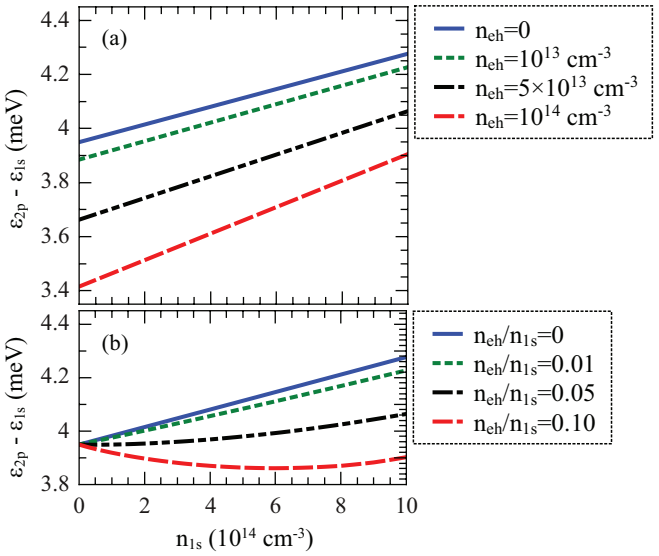

FIG. 5. (Color online) Renormalized $1s$-$2p$ transition energy for a 3D system. The exciton energy is plotted as a function of n_{1s} when the free-carrier density is (a) constant and (b) proportional to n_{1s}.

validity of our simple screening model is questionable. In the static screening model, the $2p$ state becomes unbound when the free-carrier density exceeds 2×10^9 cm^{-2} (10^{14} cm^{-3}) in a 2D (3D) system. Moreover, the behavior of the *renormalized* $2p$ state depends on the precise relationship between n_{eh} and n_{1s}. Thus interpreting the results of the present model in the high density regime would require a more thorough examination of the band edge in the presence of free-carrier screening.

V. CONCLUSION

In this paper, we have employed our excitonic dynamic equations to investigate the effects of exchange, PSF, and free-carrier screening on excitonic transitions. We find, in agreement with previous work, that the $1s$ exciton energy is slightly blue shifted due to the combined effects of PSF and exchange, and that free-carrier screening slightly increases this shift. In contrast, for a coherent exciton system (the state immediately after excitation) at moderate density, we find that free-carrier screening competes with exchange and PSF in determining the shift of the $1s$-$2p$ transition energy. Specifically, if the free-carrier density is proportional to the exciton density, the overall sign of the energy shift depends crucially on the level of screening, and we predict a redshift when $n_{eh}/n_{1s} \gtrsim 5\%$ in both 2D and 3D. Due to the lack of consensus in experiments,[9,10] a direct comparison between experimental findings and our results for this shift in the $1s$-$2p$ transition energy is difficult. We also note that the present model assumes a moderate initial excitation of the $1s$ resonance (i.e., when excitons dominate the system), whereas previous experiments have focused on the high-density regime. This was partially due to the experimental challenge of analyzing transient terahertz signals[48] from a moderately excited system, and because a primary goal of that work was to characterize the behavior of free carriers in response to an exciting optical pulse. We therefore hope to see more experimental efforts to address this problem in the future.

The factorization scheme that we have applied is chosen particularly for experiments when a resonant optical pulse is followed almost immediately by a short terahertz pulse. If the optical pulse is not resonant or the delay between the optical and terahertz pulses is larger than the dephasing times, such a factorization scheme may not be applicable and the model employed by Wang *et al.*[47] might be more appropriate. If this is the case, it should be possible to see experimentally quantitatively different behavior in the intraband peak shifts as the delay between the optical and terahertz pulses is increased beyond the interband dephasing time.

A limitation of our work is the simple static model of free-carrier screening that we employ. A dynamic screening model would require a full dynamical simulation of the EXEs [see Eqs. (10) and (B1)] and allow us to examine other many-body effects. In previous work[13] we employed the EXEs to examine the $1s$ transition energy in realistic (finite thickness) quantum wells, including coherent scattering to higher lying bound and unbound excitonic states [see Eq. (20)]. Furthermore, the EXEs can be used to describe nonlinear effects due to strong terahertz interactions [i.e., via the last term on the right-hand side of Eq. (10)]. Naturally, the utility of EXEs is not limited to the study of excitonic transitions. For any system involving terahertz interactions, the EXEs can provide a significant computational advantage over conventional dynamical models which need to exploit rotational symmetry explicitly, since the complication of terahertz-induced symmetry breaking is relegated to the exciton states. Thus the EXEs are a promising model for coherent nonlinear terahertz phenomena, such as the dynamical Franz-Keldysh effect.[58,59]

ACKNOWLEDGMENTS

We thank the Natural Sciences and Engineering Research Council of Canada for financial support. D.W. acknowledges the support from National Natural Science Foundation of China under grant No. 10904122.

APPENDIX A: FACTORIZATION SCHEME

In this Appendix, we present the justification for the factorization schemes employed to obtain the renormalized transition energies. To find the energy shifts, we need to determine the appropriate factorization scheme for the situations we are considering. To do this, we work in the coherent limit and employ the excitonic state that is created via an optical pulse followed by a terahertz pulse. For simplicity, we assume that the optical pulse is sinusoidal over the time duration ($\tau_{\rm op}$) of the pulse and is resonant with the $1s$ exciton creation energy. Similarly, we assume the terahertz pulse is sinusoidal over the time duration (τ_T) of the pulse and is resonant with the $1s$-$2p$ exciton transition energy. We are interested in the situation where there are mostly $1s$ excitons and relatively few $2p$ excitons. To treat the system in this limit, we will take the extreme limit that there is only one or fewer $2p$ excitons. Thus we treat the optical pulse nonperturbatively, but treat the terahertz pulse perturbatively.

To determine the approximate state of the system, we will ignore the non-Bosonic nature of the exciton creation and annihilation operators and will ignore the exchange and PSF terms in the Hamiltonian. This is appropriate as the corrections that arise from the exact commutation relations (8) will be one order higher in the exciton density and we are simply using this approximation in order to determine an approximate factorization for the perturbation term. We work in the interaction picture, where the unperturbed Hamiltonian is given by

$$H_o = \sum_\gamma \hbar\omega_\gamma B_\gamma^\dagger B_\gamma, \tag{A1}$$

and the optical part of the perturbation is

$$H_{\rm opt}^I = -\boldsymbol{E}_{\rm opt}(t)\cdot\sum_\gamma (C_\gamma \boldsymbol{d}_{cv} B_\gamma^\dagger e^{-i\omega_\gamma t} + \text{c.c.}). \tag{A2}$$

Now, we take the optical field to be

$$\boldsymbol{E}_{\rm opt}(t) = \boldsymbol{\mathcal{E}}_{\rm opt} e^{i\omega_{1s}t} + \text{c.c.}, \tag{A3}$$

and use the rotating wave approximation (RWA) to retain only the resonant ($1s$) terms, giving

$$H_{\rm opt}^I \simeq -\boldsymbol{\mathcal{E}}_{\rm opt}\cdot\boldsymbol{d}_{cv} C_{1s} B_{1s}^\dagger - \boldsymbol{\mathcal{E}}_{\rm opt}^*\cdot\boldsymbol{d}^*{}_{cv} C_{1s}^* B_{1s}. \tag{A4}$$

Note that in this approximation, the perturbation in the interaction picture is independent of time. Assuming the system is initially in the vacuum state ($|0\rangle$ at $t=0$), then in the interaction picture (and ignoring the terahertz pulse for now), the state for times $t \geqslant \tau_{\rm op}$ is

$$\begin{aligned}\left|\Psi_o^I\right\rangle &= \exp\left\{-iH_{\rm opt}^I\tau_p/\hbar\right\}|0\rangle \\ &= \exp\{\alpha B_{1s}^\dagger - \alpha^* B_{1s}\}|0\rangle\,,\end{aligned} \tag{A5}$$

where

$$\alpha \equiv i\boldsymbol{\mathcal{E}}_{\rm opt}\cdot\boldsymbol{d}_{cv} C_{1s}\tau_p/\hbar. \tag{A6}$$

Now, the above state is precisely the definition of a coherent state, $|\alpha\rangle_{1s}$, which satisfies

$$B_{1s}|\alpha\rangle_{1s} = \alpha|\alpha\rangle_{1s}\,. \tag{A7}$$

The number of $1s$ excitons is simply

$$\begin{aligned}\left\langle\Psi_o^I\right|B_{1s}^\dagger B_{1s}\left|\Psi_o^I\right\rangle &= \langle\alpha| B_{1s}^\dagger B_{1s}|\alpha\rangle \\ &= |\alpha|^2 \\ &\equiv N_{1s}.\end{aligned} \tag{A8}$$

Now that we have the state of the system before the terahertz pulse has been applied, let us assume that the terahertz pulse is applied at a time $t > \tau_{\rm op}$. The terahertz part of the perturbation in the interaction picture (including only the $1s$-$2p$ transitions) is given by

$$H_{\rm THz}^I = -[\boldsymbol{E}_{\rm THz}(t)\cdot\boldsymbol{G}_{2p,1s} B_{2p}^\dagger B_{1s} e^{-i\omega_T t} + \text{c.c.}], \tag{A9}$$

where

$$\omega_T \equiv \omega_{2p} - \omega_{1s}. \tag{A10}$$

Again, taking the resonant case where

$$\boldsymbol{E}_{\rm THz}(t) = \boldsymbol{\mathcal{E}}_{\rm THz} e^{i\omega_T t} + \text{c.c.}, \tag{A11}$$

and employing the RWA, we obtain

$$H_{\rm THz}^I \simeq -(\boldsymbol{\mathcal{E}}_{\rm THz}\cdot\boldsymbol{G}_{2p,1s} B_{2p}^\dagger B_{1s} + \text{c.c.}). \tag{A12}$$

If we assume that the terahertz pulse is applied for a time duration τ_T, then for times after the terahertz pulse is applied, the state is given by

$$\begin{aligned}|\Psi^I\rangle &= \exp\left(-iH_{\rm THz}^I\tau_T/\hbar\right)\left|\Psi_o^I\right\rangle \\ &= \exp(i\boldsymbol{\mathcal{E}}_{\rm THz}\cdot\boldsymbol{G}_{2p,1s} B_{2p}^\dagger B_{1s}\tau_T/\hbar)|\alpha\rangle_{1s} \\ &\quad + \exp(i\boldsymbol{\mathcal{E}}_{\rm THz}^*\cdot\boldsymbol{G}_{2p,1s}^* B_{1s}^\dagger B_{2p}\tau_T/\hbar)|\alpha\rangle_{1s}\,.\end{aligned} \tag{A13}$$

Because there are two operators in each term, this cannot be handled in the simple way that we could handle the optical perturbation (that is, it is not a coherent state). However, we will assume that the terahertz field is weak so that we can simply expand the exponential to first order in the field. Doing this, we obtain

$$\begin{aligned}|\Psi^I\rangle &\simeq (1+\Gamma_T B_{2p}^\dagger)|\alpha\rangle_{1s} \\ &= (|0\rangle_{2p} + \Gamma_T|1\rangle_{2p})|\alpha\rangle_{1s}\,,\end{aligned} \tag{A14}$$

where

$$\Gamma_T \equiv i\boldsymbol{\mathcal{E}}_{\rm THz}\cdot\boldsymbol{G}_{2p,1s}\alpha\tau_T/\hbar. \tag{A15}$$

This shows that to lowest order in the terahertz field, the total state is simply a tensor product of a $1s$ exciton state and a $2p$ exciton state (i.e., there is no entanglement of the $1s$ and $2p$ excitons).

Using the tensor product state of Eq. (A14) to evaluate expectation values, we see that to first order in Γ_t,

$$\begin{aligned}\langle B_{2p}^\dagger B_{1s}^\dagger B_{1s}\rangle &= |\alpha|^2\langle B_{2p}^\dagger\rangle \\ &= |\alpha|^2\Gamma_T^* \\ &= \langle B_{2p}^\dagger\rangle\langle B_{1s}^\dagger\rangle\langle B_{1s}\rangle.\end{aligned} \tag{A16}$$

Thus, ignoring decoherence and PSF and exchange effects, the expectation value of interest is entirely factorizable if the terahertz field is weak. Accordingly, we should simply factorize in the way that best accounts for the dephasing effects that are present in the actual system. We therefore choose our factorization such that we single out populations over coherences between different excitonic states. This procedure is similar to the RPA that is used in deriving the SBEs,[25] but is done on the level of excitonic operators rather than electron and hole operators. Importantly, it treats the intraband coherence of the excitons separately from the interband coherence.

APPENDIX B: RESULT FOR THE $1s$-$2p$ TRANSITION ENERGY FROM INTRABAND EXE

In this Appendix, we calculate this shift in the $1s$-$2p$ exciton transition energy using the dynamic EXE for the intraband coherence function, $\langle B_\mu^\dagger B_\nu\rangle$. We will show that this shift is identical to what one would obtain using the interband coherence functions for the two excitonic states involved in the transition. Although this may seem redundant, we show that the equivalence only occurs in the macroscopic limit ($V \gg a_o^D$ for a D-dimensional system).

Neglecting the terahertz and optical interaction terms (for simplicity), the EXE for the intraband coherence function is[13]

$$i\hbar\frac{d}{dt}\langle B_\mu^\dagger B_\nu\rangle + (E_\mu - E_\nu - i\hbar/T_{\mu,\nu})\langle B_\mu^\dagger B_\nu\rangle = 2\sum_{\{\gamma_j\}} S^{\mu\nu}_{\gamma_1\gamma_2\gamma_3\gamma_4}\langle B_{\gamma_1}^\dagger B_{\gamma_2}^\dagger B_{\gamma_3} B_{\gamma_4}\rangle, \tag{B1}$$

where $T_{\mu,\nu}$ is the intraband dephasing time when $\mu \neq \nu$, and is the exciton population decay time when $\mu = \nu$. The coefficient

$$S^{\mu\nu}_{\gamma_1\gamma_2\gamma_3\gamma_4} = W^{\mu\nu}_{\gamma_1\gamma_2\gamma_3\gamma_4} + U^{\mu\nu}_{\gamma_1\gamma_2\gamma_3\gamma_4} \tag{B2}$$

is analogous to the R coefficient appearing in the interband EXE (20). The components of the S coefficient,

$$W^{\mu\nu}_{\gamma_1\gamma_2\gamma_3\gamma_4} = \sum_{\boldsymbol{k},\boldsymbol{p},\boldsymbol{q}} (V_{\boldsymbol{p}-\boldsymbol{k}} - V_{\boldsymbol{q}-\boldsymbol{k}})\varphi_{\boldsymbol{p}}^{\mu}\varphi_{\boldsymbol{q}}^{\nu *}\varphi_{\boldsymbol{p}}^{\gamma_1 *}\varphi_{\boldsymbol{k}}^{\gamma_2 *}\varphi_{\boldsymbol{k}}^{\gamma_3}\varphi_{\boldsymbol{q}}^{\gamma_4} \times (1-\delta_{\boldsymbol{p},\boldsymbol{k}})(1-\delta_{\boldsymbol{q},\boldsymbol{k}}), \tag{B3}$$

$$U^{\mu\nu}_{\gamma_1\gamma_2\gamma_3\gamma_4} = -\sum_{\boldsymbol{k},\boldsymbol{p},\boldsymbol{q}} \left(\varphi_{\boldsymbol{p}}^{\mu}\varphi_{\boldsymbol{q}}^{\nu *}V_{\boldsymbol{p}-\boldsymbol{k}} - \varphi_{\boldsymbol{k}}^{\mu}\varphi_{\boldsymbol{p}}^{\nu *}V_{\boldsymbol{q}-\boldsymbol{p}}\right) \times \varphi_{\boldsymbol{k}}^{\gamma_1 *}\varphi_{\boldsymbol{p}}^{\gamma_2 *}\varphi_{\boldsymbol{p}}^{\gamma_3}\varphi_{\boldsymbol{q}}^{\gamma_4}(1-\delta_{\boldsymbol{p},\boldsymbol{k}})(1-\delta_{\boldsymbol{p},\boldsymbol{q}}), \tag{B4}$$

are due to exchange and PSF, respectively. We will now determine the relationship between the S coefficients and the R coefficients. Focusing on the exchange component, we have

$$\begin{aligned} W^{\mu,\nu}_{\gamma_1,\gamma_2,\gamma_3,\gamma_4} = {} & \delta_{\nu,\gamma_4}\sum_{\boldsymbol{k},\boldsymbol{p}}(1-\delta_{\boldsymbol{p}\boldsymbol{k}})V_{\boldsymbol{p}-\boldsymbol{k}}\varphi_{\boldsymbol{p}}^{\mu}\varphi_{\boldsymbol{p}}^{\gamma_1 *}\varphi_{\boldsymbol{k}}^{\gamma_2 *}\varphi_{\boldsymbol{k}}^{\gamma_3} \\ & -\sum_{\boldsymbol{p},\boldsymbol{q}}(1-\delta_{\boldsymbol{p}\boldsymbol{q}})V_{\boldsymbol{p}-\boldsymbol{q}}\varphi_{\boldsymbol{p}}^{\mu}\varphi_{\boldsymbol{q}}^{\nu *}\varphi_{\boldsymbol{p}}^{\gamma_1 *}\varphi_{\boldsymbol{k}}^{\gamma_2 *}\varphi_{\boldsymbol{k}}^{\gamma_3}\varphi_{\boldsymbol{q}}^{\gamma_4} \\ & -\delta_{\mu,\gamma_1}\sum_{\boldsymbol{k},\boldsymbol{q}}(1-\delta_{\boldsymbol{q}\boldsymbol{k}})V_{\boldsymbol{q}-\boldsymbol{k}}\varphi_{\boldsymbol{q}}^{\nu *}\varphi_{\boldsymbol{k}}^{\gamma_2 *}\varphi_{\boldsymbol{k}}^{\gamma_3}\varphi_{\boldsymbol{q}}^{\gamma_4} \\ & +\sum_{\boldsymbol{p},\boldsymbol{q}}(1-\delta_{\boldsymbol{q}\boldsymbol{p}})V_{\boldsymbol{q}-\boldsymbol{p}}\varphi_{\boldsymbol{p}}^{\mu}\varphi_{\boldsymbol{q}}^{\nu *}\varphi_{\boldsymbol{p}}^{\gamma_1 *}\varphi_{\boldsymbol{k}}^{\gamma_2 *}\varphi_{\boldsymbol{k}}^{\gamma_3}\varphi_{\boldsymbol{q}}^{\gamma_4}, \end{aligned} \tag{B5}$$

where we have used

$$\sum_{\boldsymbol{k}}\varphi_{\boldsymbol{k}}^{\gamma *}\varphi_{\boldsymbol{k}}^{\gamma'} = \delta_{\gamma,\gamma'}, \tag{B6}$$

which follows from the orthonormality of the excitonic states.

Comparing Eq. (B5) to Eq. (12), we see that

$$\begin{aligned} W^{\mu\nu}_{\gamma_1\gamma_2\gamma_3\gamma_4} = {} & \delta_{\nu,\gamma_4}X^{\mu}_{\gamma_1\gamma_2\gamma_3} - \delta_{\mu,\gamma_1}X^{\nu *}_{\gamma_4\gamma_3\gamma_2} \\ & -\sum_{\boldsymbol{p},\boldsymbol{q}}(1-\delta_{\boldsymbol{p}\boldsymbol{q}})V_{\boldsymbol{p}-\boldsymbol{q}}\varphi_{\boldsymbol{p}}^{\mu}\varphi_{\boldsymbol{q}}^{\nu *}\varphi_{\boldsymbol{p}}^{\gamma_1 *}\varphi_{\boldsymbol{q}}^{\gamma_2 *}\varphi_{\boldsymbol{q}}^{\gamma_3}\varphi_{\boldsymbol{q}}^{\gamma_4} \\ & +\sum_{\boldsymbol{p},\boldsymbol{q}}(1-\delta_{\boldsymbol{q}\boldsymbol{p}})V_{\boldsymbol{q}-\boldsymbol{p}}\varphi_{\boldsymbol{p}}^{\mu}\varphi_{\boldsymbol{q}}^{\nu *}\varphi_{\boldsymbol{p}}^{\gamma_1 *}\varphi_{\boldsymbol{p}}^{\gamma_2 *}\varphi_{\boldsymbol{p}}^{\gamma_3}\varphi_{\boldsymbol{q}}^{\gamma_4}. \end{aligned} \tag{B7}$$

Now, it can be shown that the last two terms in this equation scale as $(L/a_o)^{-2D}$, so we may write

$$W^{\mu\nu}_{\gamma_1\gamma_2\gamma_3\gamma_4} = \delta_{\nu,\gamma_4}X^{\mu}_{\gamma_1\gamma_2\gamma_3} - \delta_{\mu,\gamma_1}X^{\nu *}_{\gamma_4\gamma_3\gamma_2} + \mathcal{O}[(L/a_o)^{-2D}], \tag{B8}$$

where the last term is negligible if the system is sufficiently large. Similarly, one finds

$$U^{\mu\nu}_{\gamma_1\gamma_2\gamma_3\gamma_4} = \delta_{\nu,\gamma_4}P^{\mu}_{\gamma_1\gamma_2\gamma_3} - \delta_{\mu,\gamma_1}P^{\nu *}_{\gamma_4\gamma_3\gamma_2} + \mathcal{O}[(L/a_o)^{-2D}], \tag{B9}$$

so we approximate

$$S^{\mu\nu}_{\gamma_1\gamma_2\gamma_3\gamma_4} \simeq \delta_{\nu,\gamma_4}R^{\mu}_{\gamma_1\gamma_2\gamma_3} - \delta_{\mu,\gamma_1}R^{\nu *}_{\gamma_4\gamma_3\gamma_2}. \tag{B10}$$

Thus, in the limit of a macroscopic system, Eq. (B1) may be written as

$$i\hbar\frac{d}{dt}\langle B_\mu^\dagger B_\nu\rangle + (E_\mu - E_\nu)\langle B_\mu^\dagger B_\nu\rangle = 2\sum_{\{\gamma_j\}}\left(R^{\mu}_{\gamma_1\gamma_2\gamma_3}\langle B_{\gamma_1}^\dagger B_{\gamma_2}^\dagger B_{\gamma_3} B_\nu\rangle - R^{\nu *}_{\gamma_3\gamma_2\gamma_1}\langle B_\mu^\dagger B_{\gamma_1}^\dagger B_{\gamma_2} B_{\gamma_3}\rangle\right). \tag{B11}$$

Now, we are interested in the $1s$-$2p$ excitonic transition, where $\mu = 2p$ and $\nu = 1s$. Also, as we did in the interband case, we consider only the resonant response and only the terms where three of the operators are $1s$ operators. We then obtain

$$i\hbar\frac{d}{dt}\langle B_{2p}^\dagger B_{1s}\rangle + (E_{2p} - E_{1s})\langle B_{2p}^\dagger B_{1s}\rangle = 2\left(R^{2p}_{2p1s1s} + R^{2p}_{1s,2p,1s} - R^{1s*}_{1s,1s,1s}\right)\langle B_{2p}^\dagger B_{1s}^\dagger B_{1s} B_{1s}\rangle. \tag{B12}$$

Following the discussion of Appendix A, we see that

$$\begin{aligned} \langle B_{2p}^\dagger B_{1s}^\dagger B_{1s} B_{1s}\rangle &= \alpha\,|\alpha|^2\,\langle B_{2p}^\dagger\rangle \\ &= \alpha\,|\alpha|^2\,\Gamma_T^* \\ &= \langle B_{2p}^\dagger\rangle\langle B_{1s}^\dagger\rangle\langle B_{1s}\rangle\langle B_{1s}\rangle. \end{aligned} \tag{B13}$$

Again, if we single out the populations and apply the factorization

$$\langle B_{2p}^\dagger B_{1s}^\dagger B_{1s} B_{1s}\rangle \to \langle B_{2p}^\dagger B_{1s}\rangle\langle B_{1s}^\dagger B_{1s}\rangle \tag{B14}$$

to Eq. (B12), we see that the energy shift for $1s$-$2p$ transition energy is given by

$$\Delta E_{2p-1s} = 2\left(R^{1s*}_{1s,1s,1s} - R^{2p}_{2p1s1s} - R^{2p}_{1s,2p,1s}\right)N_{1s}. \tag{B15}$$

Since the R coefficients are real (see Appendix C), this energy shift may also be written as

$$\Delta E_{2p-1s} = (\varepsilon_{2p} - E_{2p}) - (\varepsilon_{1s} - E_{1s}), \tag{B16}$$

where the individual renormalized exciton energies $(\varepsilon_{1s},\varepsilon_{2p})$ are given by the interband result, Eq. (24).

APPENDIX C: EVALUATION OF THE R COEFFICIENTS

In this Appendix, we outline the approaches used to calculate the R coefficients for screened and unscreened systems. The R coefficients involve multidimensional integrals that can be evaluated analytically in the absence of screening. However, when $\kappa \neq 0$, the integrals must be evaluated numerically. To verify our screened results, we compare these numerical results to the analytic results in the limit that $\kappa \to 0$.

1. Analytic evaluation of unscreened coefficients

a. Coefficients for a 2D system

For the two-dimensional Coulomb matrix elements, we use the cylindrical expansion[60]

$$\frac{1}{|\boldsymbol{k}-\boldsymbol{p}|}=\sum_{m=-\infty}^{\infty}\int_0^\infty du e^{im(\phi_p-\phi_k)}J_m(up)J_m(uk). \quad \text{(C1)}$$

The angular integrals for the X and P coefficients terminate this summation by fixing the value of m. Thus the coefficients are given by infinite integrals involving Bessel functions. For example, the dimensionless exchange coefficient is given by

$$\overline{X}^{1s}_{1s,1s,1s}=4\iint_0^\infty dydu\frac{J_0(yu)u}{(1+u^2)^3}\int_0^\infty dv\frac{J_0(yv)v}{(1+v^2)^3}, \quad \text{(C2)}$$

where $u\equiv a_0k$; $v\equiv a_0p$. The integrals for the $X^{1s}_{1s,1s,1s}$ and $P^{1s}_{1s,1s,1s}$ coefficients follow immediately from tabulated results,[61] and we obtain

$$\overline{R}^{1s}_{1s1s1s}=\left(\frac{315\pi^2}{2^{13}}-\frac{1}{2}\right)\simeq -0.1205. \quad \text{(C3)}$$

It is straightforward to evaluate the integrals for the $\overline{X}^{2p}_{2p,1s,1s}$, $\overline{P}^{2p}_{2p,1s,1s}$, and $\overline{P}^{2p}_{1s,2p,1s}$ coefficients using tabulated integrals and relations for Bessel functions.[61,62] However, the $\overline{X}^{2p}_{1s,2p,1s}$ coefficient involves the integral

$$\int_0^\infty du\frac{u^2J_1(yu)}{(1+u^2/9)^{\frac{3}{2}}(1+u^2)^{\frac{5}{2}}}, \quad \text{(C4)}$$

for which there is no simple result. In principle, the contour method employed by Watson[50] to evaluate Hankel's integral,

$$\int_0^\infty dx\frac{J_\lambda(ax)x^\mu}{(x^2+b^2)^\nu}, \quad \text{(C5)}$$

could be generalized to the case of Eq. (C4). However, the resulting expression becomes so complicated that it is preferable to evaluate $\overline{X}^{2p}_{1s,2p,1s}$ as an infinite series of hypergeometric functions, similar to the approach we use below to calculate the 3D coefficients (see Sec. C 1b).

The numerical values for all of the exchange and PSF coefficients are given in Table I. As is discussed in part 2 of this Appendix, for a screened Coulomb interaction, these coefficients must be calculated numerically. We have used our numerical results to calculate these coefficients in the limit $\kappa\to 0$, and we find in all cases that the difference between the numerical and analytic results is less than 0.1%.

b. Coefficients for a 3D system

For a three-dimensional system, we employ the spherical expansion,[60]

$$\frac{1}{|\boldsymbol{k}-\boldsymbol{p}|^2}=(4\pi)^2\sum_{\substack{l,m\\ l',m'}}\frac{1}{(2l+1)(2l'+1)}\frac{[\min(k,p)]^{l+l'}}{[\max(k,p)]^{l+l'+2}}$$
$$\times Y_l^m(\Omega_k)Y_l^{m*}(\Omega_p)Y_{l'}^{m'*}(\Omega_k)Y_{l'}^{m'}(\Omega_p), \quad \text{(C6)}$$

where P coefficients eliminate the primed summations, and the sum over m is simply a constant that depends on l. This reduces the coefficients to a summation of double integrals with respect to k and p. Since the expansion of Eq. (C6) depends on the relative magnitudes of k and p, it is necessary to break up the integration regions to make the integrands explicit. For example, the $X^{1s}_{1s,1s,1s}$ coefficient may be written as

$$\overline{X}^{1s}_{1s,1s,1s}=\frac{2^{10}}{\pi^2}\sum_{l=0}^{\infty}\frac{A_l+B_l}{(2l+1)}, \quad \text{(C7)}$$

where

$$A_l=\int_0^\infty du\frac{u^{-2l}}{(1+u^2)^4}\int_0^u dv\frac{v^{2l+2}}{(1+v^2)^4}, \quad \text{(C8)}$$
$$B_l=\int_0^\infty du\frac{u^{2l+2}}{(1+u^2)^4}\int_u^\infty dv\frac{v^{-2l}}{(1+v^2)^4}, \quad \text{(C9)}$$

and $u\equiv a_0k$, $v\equiv a_0p$. Similar expressions can be obtained for the other coefficients, and we refer to the integrals in the summation as *expansion integrals*. It is worthwhile to note that the expansion integrals can be evaluated analytically. Defining $t\equiv(v/u)^2$, the A_l integral becomes

$$A_l=\frac{1}{2}\int_0^\infty du\frac{u^3}{(1+u^2)^4}\int_0^1 dt\frac{t^{l+\frac{1}{2}}}{(1+tu^2)^4}. \quad \text{(C10)}$$

The integrand is non-negative, and the double integral clearly converges $\forall l\geqslant 0$. Thus we may change the order of integration and use the tabulated result[61]

$$\int_0^\infty dx x^{\kappa-1}(1+\alpha x^q)^{-\mu}(1+\beta x^q)^{-\nu}$$
$$=\frac{\alpha^{-\frac{\kappa}{q}}\Gamma\left(\frac{\kappa}{q}\right)\Gamma\left(\mu+\nu-\frac{\kappa}{q}\right)}{q\Gamma(\mu+\nu)}{}_2F_1\left(\nu,\frac{\kappa}{q};\mu+\nu;1-\frac{\beta}{\alpha}\right), \quad \text{(C11)}$$

where ${}_pF_q$ is a generalized hypergeometric series. This yields

$$A_l=\frac{1}{168}\int_0^1 dt t^{l+\frac{1}{2}}{}_2F_1(4,2;8;1-t)$$
$$={}_3F_2\left(2,4,1;8,\tfrac{5}{2}+l;1\right)\Big/84(3+2l). \quad \text{(C12)}$$

A similar calculation shows that $B_l=A_l$, hence

$$\bar{X}^{1s}_{1s,1s,1s}=\frac{2^9}{21\pi^2}\sum_{l=0}^{\infty}\frac{{}_3F_2\left(2,4,1;8,\frac{5}{2}+l;1\right)}{(2l+1)(2l+3)}. \quad \text{(C13)}$$

The hypergeometric series can be reduced to a rational expression for each l using computer algebra software; for example,

$$A_0=\frac{5\pi^2}{2048}-\frac{1}{60}\simeq 0.007429. \quad \text{(C14)}$$

For large l, the hypergeometric series approaches the limit

$$\lim_{l\to\infty}{}_3F_2\left(2,4,1;8,\frac{5}{2}+l;1\right)=1. \quad \text{(C15)}$$

Thus, if we include $L \gg 1$ terms in the summation for $\bar{X}^{1s}_{1s1s1s}$, the absolute error is approximately

$$\varepsilon_L = \frac{2^8 {}_3F_2\left(2,4,1;8,\frac{5}{2}+L;1\right)}{21(2L+1)\pi^2}. \tag{C16}$$

For $L = 100$, the $\bar{X}^{1s}_{1s,1s,1s}$ coefficient is found to be

$$\bar{X}^{1s}_{1s,1s,1s} \simeq 2.077 + \varepsilon_{100} = 2.083. \tag{C17}$$

This calculation is rather tedious, however, and it is more efficient to evaluate the expansion integrals numerically. To do this, we first transform the expansion integrals to double integrals with constant limits, as in Eq. (C10). These integrals can be rapidly evaluated to high precision using standard numerical techniques. The results for the X and P coefficients relevant to the $1s$-$2p$ transition are summarized in Table I. Again, these values are in agreement with the results obtained by purely numerical evaluation of the coefficients in the limit of zero screening to better than 0.1%.

2. Influence of screening on the R coefficients

The statically screened Coulomb matrix elements [see Eqs. (28) and (29)] do not admit convenient expansions in terms of orthogonal functions. Rather, the integrals for the X and P coefficients must be evaluated numerically when $\kappa \neq 0$. Apart from a removable cusp at $\boldsymbol{k} = \boldsymbol{p}$, the integrands are smooth to infinite order. Thus the coefficients may be evaluated using multidimensional quadrature, and we employ Smolyak's construction of sparse grids[63] to reduce the computation time. The calculation is further enhanced using an adaptive strategy.[64] Figure 6 shows the effect of screening on the R coefficients relevant to the $1s$-$2p$ transition energy. As mentioned in the main text, the dependence of these coefficients on the free-carrier density is quite weak.

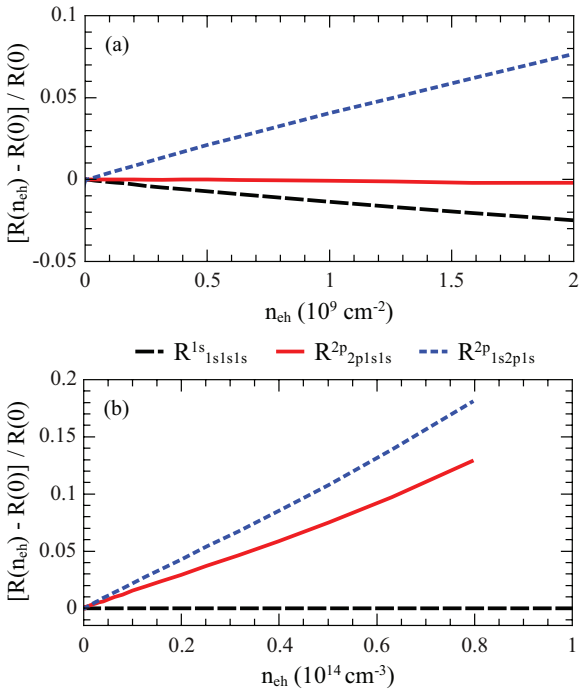

FIG. 6. (Color online) Influence of screening on the R coefficients, relative to unscreened values, in (a) 2D and (b) 3D systems.

*dignam@physics.queensu.ca

[1] J. Shah, *Ultrafast Spectroscopy of Semiconductors and Semiconductor Nanostructures* (Springer-Verlag, Berlin, 1996).
[2] L. Yang and M. M. Dignam, Phys. Rev. B **73**, 035334 (2006).
[3] N. Peyghambarian, H. M. Gibbs, J. L. Jewell, A. Antonetti, A. Migus, D. Hulin, and A. Mysyrowicz, Phys. Rev. Lett. **53**, 2433 (1984).
[4] M. Choi, K. C. Je, S. Y. Yim, and S. H. Park, Phys. Rev. B **70**, 085309 (2004).
[5] D. Hulin, A. Mysyrowicz, A. Antonetti, A. Migus, W. T. Masselink, H. Morkoc, H. M. Gibbs, and N. Peyghambarian, Phys. Rev. B **33**, 4389 (1986).
[6] F. Rossi and T. Kuhn, Rev. Mod. Phys. **74**, 895 (2002).
[7] J. Feldmann, K. Leo, J. Shah, D. A. B. Miller, J. E. Cunningham, T. Meier, G. vonPlessen, A. Schulze, P. Thomas, and S. Schmitt-Rink, Phys. Rev. B **46**, 7252 (1992).
[8] D. B. Turner, P. Wen, D. H. Arias, K. A. Nelson, H. Li, G. Moody, M. E. Siemens, and S. T. Cundiff, Phys. Rev. B **85**, 201303 (2012).
[9] R. Huber, R. A. Kaindl, B. A. Schmid, and D. S. Chemla, Phys. Rev. B **72**, 161314 (2005).
[10] T. Grunwald *et al.*, Phys. Stat. Sol. C **6**, 500 (2009).
[11] T. Suzuki and R. Shimano, Phys. Rev. Lett. **103**, 057401 (2009).
[12] K. H. Schlaad, C. Weber, J. Cunningham, C. V. Hoof, G. Borghs, G. Weimann, W. Schlapp, H. Nickel, and C. Klingshirn, Phys. Rev. B **43**, 4268 (1991).
[13] D. Wang and M. M. Dignam, Phys. Rev. B **79**, 165320 (2009).
[14] G. Manzke, Q. Y. Peng, K. Henneberger, U. Neukirch, K. Hauke, K. Wundke, J. Gutowski, and D. Hommel, Phys. Rev. Lett. **80**, 4943 (1998).
[15] R. Shimano and T. Suzuki, Phys. Stat. Sol. C **8**, 1153 (2011).
[16] J. Kasprzak *et al.*, Nature (London) **443**, 409 (2006).
[17] A. Amo *et al.*, Nature (London) **457**, 291 (2009).
[18] A. Amo *et al.*, Nat. Phys. **5**, 805 (2009).
[19] A. Kavokin, Phys. Status Solidi B **247**, 1898 (2010).
[20] H. Deng and Y. Yamamoto, Rev. Mod. Phys. **82**, 1489 (2010).
[21] H. M. Gibbs, G. Khitrova, and S. W. Koch, Nat. Photon. **5**, 273 (2011).
[22] X. Zhu, P. B. Littlewood, M. S. Hybertsen, and T. M. Rice, Phys. Rev. Lett. **74**, 1633 (1995).
[23] P. R. Eastham *et al.*, J. Phys. Condens. Matter **16**, S3597 (2004).
[24] K. Kamide and T. Ogawa, Phys. Rev. B **83**, 165319 (2011).
[25] H. Haug and S. W. Koch, *Quantum Theory of the Optical and Electronic Properties of Semiconductors*, 4th ed. (World Scientific, Singapore, 1994).

[26]G. D. Mahan, *Many-Particle Physics*, 3rd ed. (Kluwer Academic, New York, 2000).
[27]M. Lindberg and S. W. Koch, Phys. Rev. B **38**, 3342 (1988).
[28]D. Wang, Ph.D. thesis, Queen's University, 2008, http://hdl.handle.net/1974/1593.
[29]V. M. Axt, G. Bartels, and A. Stahl, Phys. Rev. Lett. **76**, 2543 (1996).
[30]M. Kira and S. W. Koch, Eur. Phys. J. D **36**, 143 (2005).
[31]V. M. Axt and A. Stahl, Z. Phys. B. **93**, 195 (1994).
[32]K. Kamide and T. Ogawa, Phys. Rev. Lett. **105**, 056401 (2010).
[33]Takayama, N. H. Kwong, I. Rumyantsev, M. Kuwata-Gonokami, and R. Binder, Eur. Phys. J. B **25**, 445 (2002).
[34]Z. S. Yang, N. H. Kwong, R. Takayama, and R. Binder, Europhys. Lett. **69**, 417 (2005).
[35]M. Combescot and O. Beebeder-Matibet, Europhys. Lett. **62**, 140 (2003).
[36]M. Combescot, O. Betbeder-Matibeta, and F. Dubin, Phys. Rep. **463**, 215 (2008).
[37]M. Hawton and D. Nelson, Phys. Rev. B **57**, 4000 (1998).
[38]M. M. Dignam and M. Hawton, Phys. Rev. B **67**, 035329 (2003).
[39]M. Hawton and M. M. Dignam, Phys. Rev. Lett. **91**, 267402 (2003).
[40]L. Yang, B. Rosam, J.-M. Lachaine, K. Leo, and M. M. Dignam, Phys. Rev. B **69**, 165310 (2004).
[41]D. Wang, M. Hawton, and M. M. Dignam, Phys. Rev B **76**, 115311 (2007).
[42]S. Schmitt-Rink, D. S. Chemla, and D. A. B. Miller, Phys. Rev. B **32**, 6601 (1985).
[43]T. Hiroshima, Phys. Rev. B **40**, 3862 (1989).
[44]S. Portolan, O. DiStefano, S. Savasta, F. Rossi, and R. Girlanda, Phys. Rev B **77**, 195305 (2008).
[45]L. Yang and M. M. Dignam, Phys. Rev. B **73**, 075319 (2006).
[46]D. Wang, A. Zhang, L. Yang, and M. M. Dignam, Phys. Rev. B **77**, 115307 (2008).
[47]D. Wang, X. Lei, and Z. Wu, J. Phys.: Condens. Matter **23**, 345801 (2011).
[48]R. A. Kaindl, D. Hagele, M. A. Carnahan, and D. S. Chemla, Phys. Rev. B **79**, 045320 (2009).
[49]J. Lee, H. N. Spector, and P. Melman, J. Appl. Phys. **58**, 1893 (1985).
[50]G. N. Watson, *A Treatise on the Theory of Bessel Functions* (Cambridge University Press, Cambridge, UK, 1995).
[51]F. Stern and W. E. Howard, Phys. Rev. **163**, 816 (1967).
[52]T. Ando, A. B. Fowler, and F. Stern, Rev. Mod. Phys. **54**, 437 (1982).
[53]M. E. Portnoi and I. Galbraith, Phys. Rev. B **60**, 5570 (1999).
[54]T. Yoshioka and K. Asano, Phys. Rev. B **86**, 115314 (2012).
[55]G. W. Fehrenbach, W. Schafer, J. Treusch, and R. G. Ulbrich, Phys. Rev. Lett. **49**, 1281 (1982).
[56]S. Nojima, Phys. Rev. B **51**, 11124 (1995).
[57]As discussed in previous work,[47] phase coherence is another factor that can determine if the $1s$-$2p$ transitions is red or blue shifted.
[58]C. J. Dent, B. N. Murdin, and I. Galbraith, Phys. Rev. B **67**, 165312 (2003).
[59]S. Hughes and D. S. Citrin, Phys. Rev. B **59**, R5288 (1999).
[60]J. D. Jackson, *Classical Electrodynamics*, 3rd ed. (Wiley, New York, 1999).
[61]I. Gradshteyn and I. M. Ryzhik, *Table of Integrals, Series, and Products*, 5th ed. (Academic Press, New York, 1994).
[62]M. Abramovitz and I. A. Stegun, *Handbook of Mathematical Functions*, National Bureau of Standards, Applied Mathematics Series 55, 10th ed. (1972).
[63]S. A. Smolyak, Soviet Math. Dokl. **4**, 240 (1963).
[64]P. V. Dooren and L. D. Ridder, J. Comput. Appl. Math. **2**, 207 (1976).